Supporting Information for

One-Pot Synthesis of Flower-Like Bi_2S_3 Nanoparticles for Spectral CT imaging and Photothermal Therapy in Vivo

Cai Zhang,[‡a*] Li Zhou,[‡b] Jing Zhang,[c] Rui Dai,[d] Pengrui Zhuang,[e] Zhaoxiang Ye[a*]

a. Department of Radiology, Tianjin Medical University Cancer Institute and Hospital, National Clinical Research Centre of Cancer, Key Laboratory of Cancer Prevention and Therapy, Tianjin 300060, China.
b. Department of Radiology, Tianjin Medical University General Hospital, Tianjin 300052, China.
c. Department of Radiology, West China Hospital of Sichuan University, Chengdu 610044, China.
d. Department of Echocardiography, Tianjin Children's Hospital, Tianjin 300074, China.
e. Department of Radiology, Tianjin Medical University Second Hospital, Tianjin 300201, China.
‡These authors contributed equally to this work.

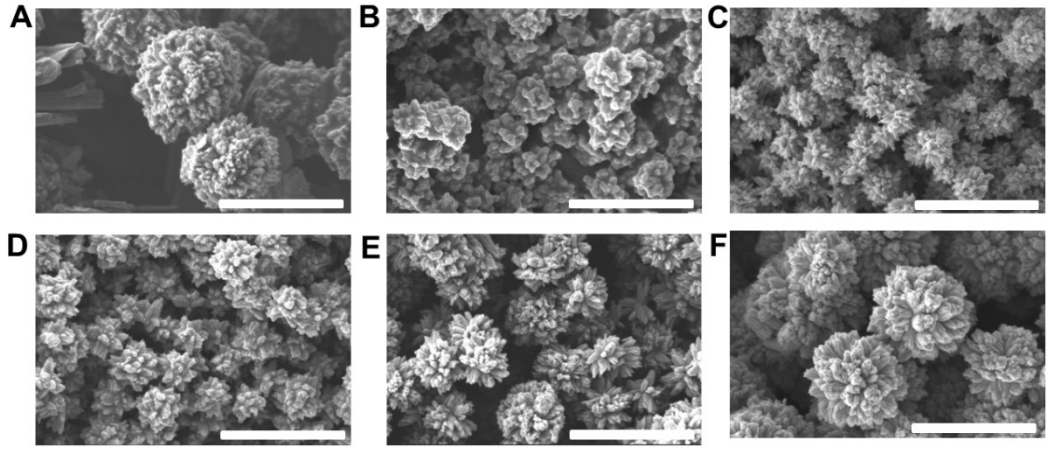

Fig. S1 SEM of the Bi_2S_3 NPs, scale bar: 1μm.

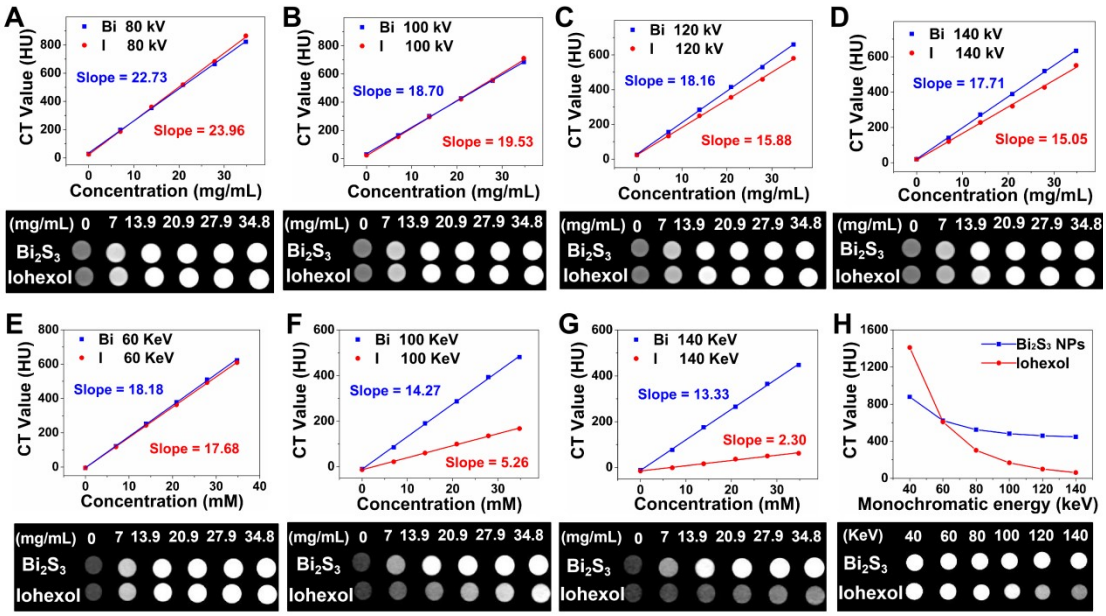

Fig. S2 CT signal curves and CT images of Bi_2S_3 NPs with various concentrations (7-34.8 mg/mL Bi_2S_3 NPs or iohexol) under different tube voltages and monochromatic energies. CT signal curves and CT images of Bi_2S_3 NPs obtained at the tube voltage of 80 kV (A), 100 kV (B), 120 kV (C) and 140 kV (D). CT value curves and spectral CT images of Bi_2S_3 NPs and iohexol at the monochromatic energies of 60 KeV (E), 100 KeV (F) and 140 KeV (G). (H) The CT values and monochromatic spectral CT images of Bi_2S_3 NPs (34.8 mg/mL) and iohexol (34.8 mg/mL) at different monochromatic energies.

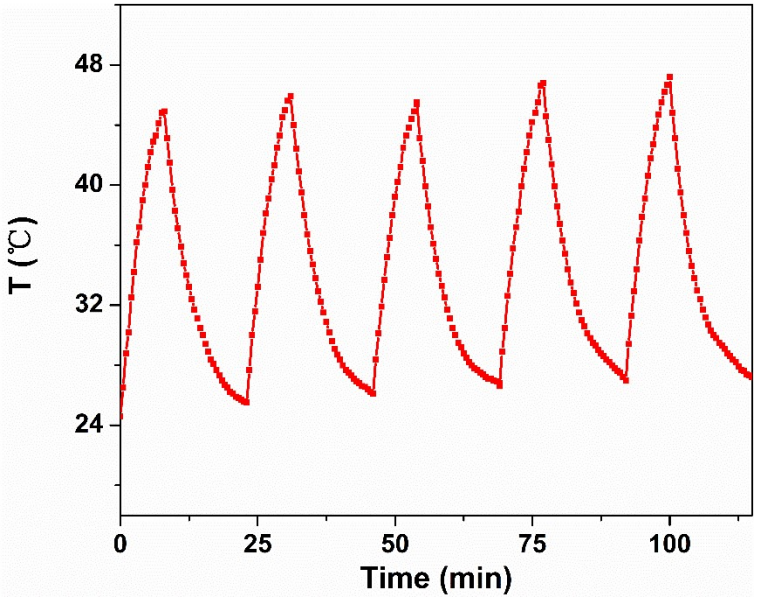

Fig. S3 The photothermal heating stability assessment by five cycles of laser on/off operation (Laser on: 8 min, Laser off: 15 min).

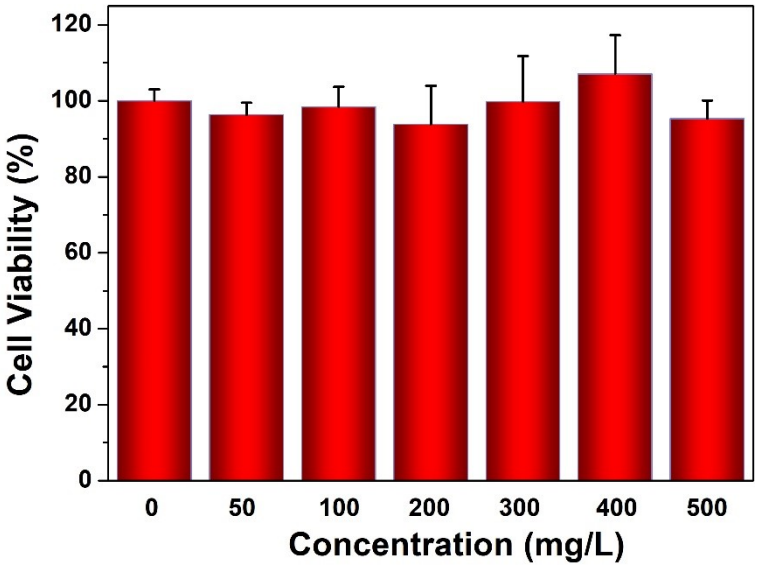

Fig. S4 The viabilities of 3T3-L1 cells after incubated with different concentrations of Bi_2S_3 NPs by a MTT assay.

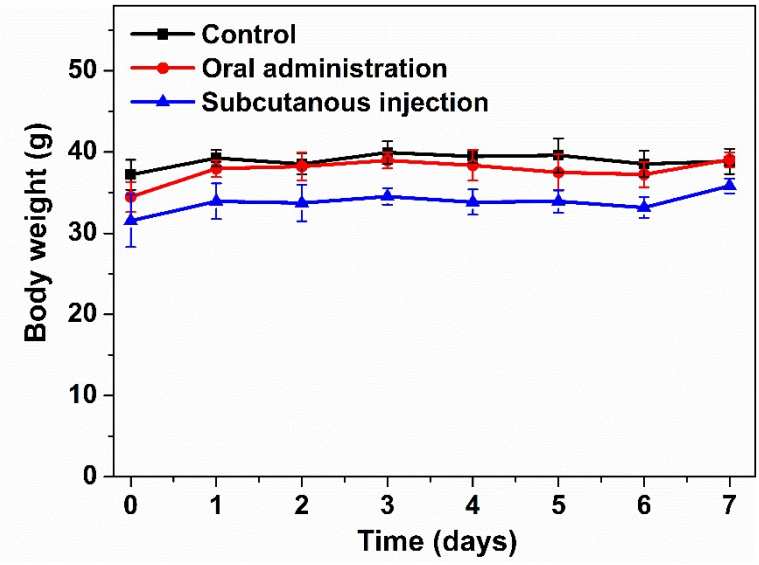

Fig. S5 Body weight changes of the mice treated with Bi_2S_3 NPs by subcutaneous injection or oral administration for 7 days, and the mice without any treatment were set as control.

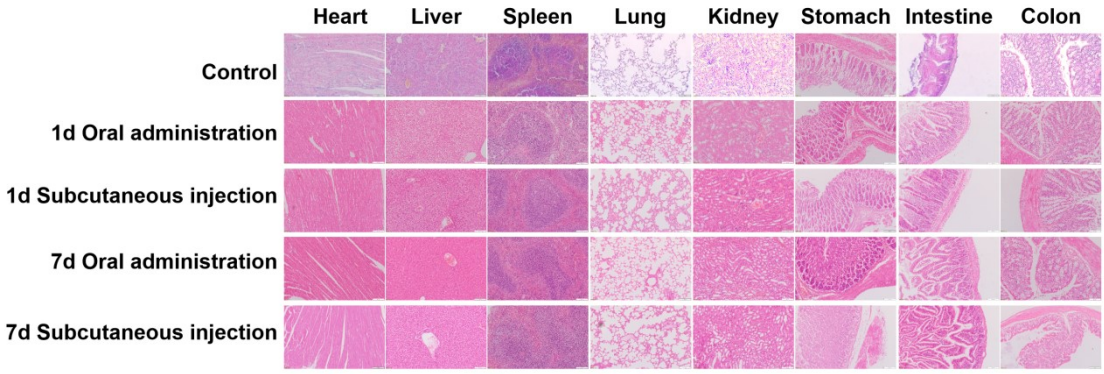

Fig. S6 Histopathological analysis of the major organs (heart, liver, spleen, lung, kidney, stomach, intestine and colon) from the mice was conducted after subcutaneous injection or oral administration with Bi_2S_3 NPs for1 or 7 days, and the mice without any treatments were set as control.

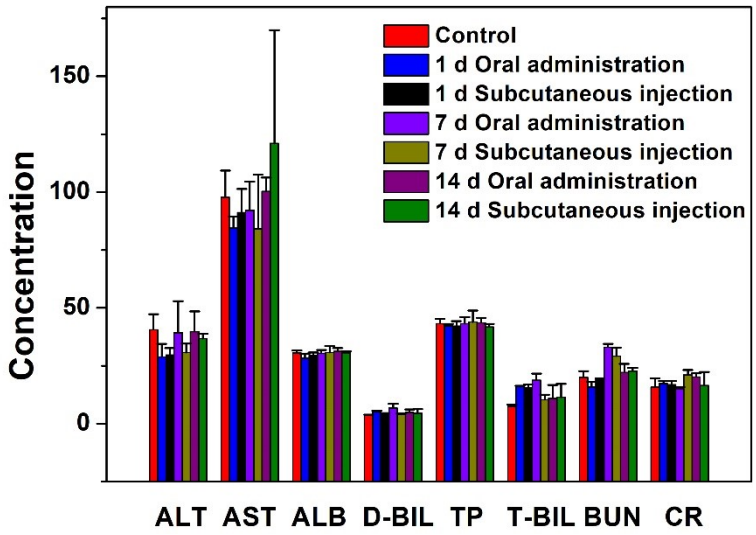

Fig. S7 Biochemical analysis of mice at different time points after subcutaneous injection or oral administration of Bi_2S_3 NPs, and the mice without any treatment were set as the control group.

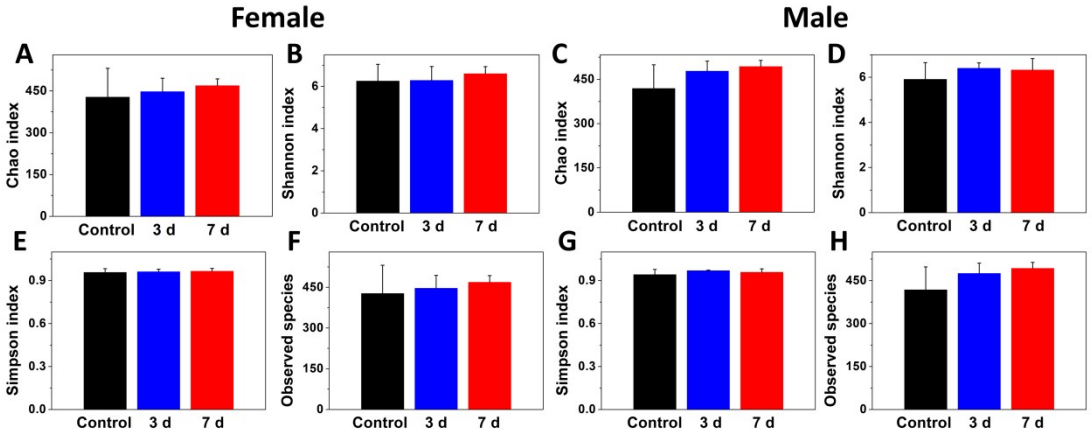

Fig. S8 Alpha analysis of the diversity of gut microbiota in female/male mice at different time points (3 and 7 days) after oral administration of Bi_2S_3 NPs. Untreated mice served as control group. The gut microbiota was evaluated by the indexes of Chao, Shannon, Simpson, and Observed species (A–H).

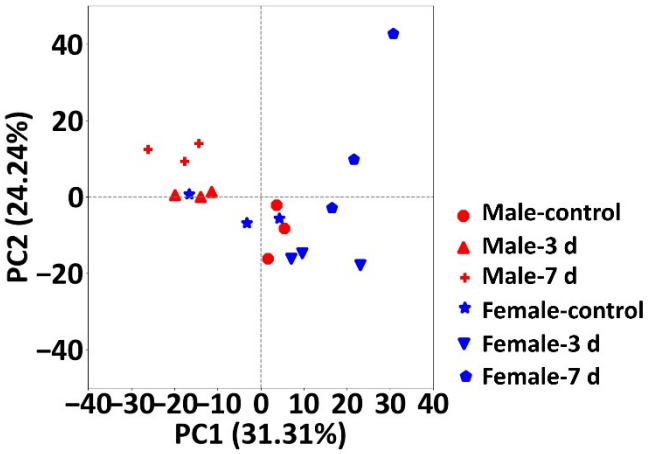

Fig. S9 Principal component analysis of the diversity of gut microbiota in female/male mice at different time points (3 and 7 days) after oral administration of Bi_2S_3 NPs. Mice without any treatment were set as the control.

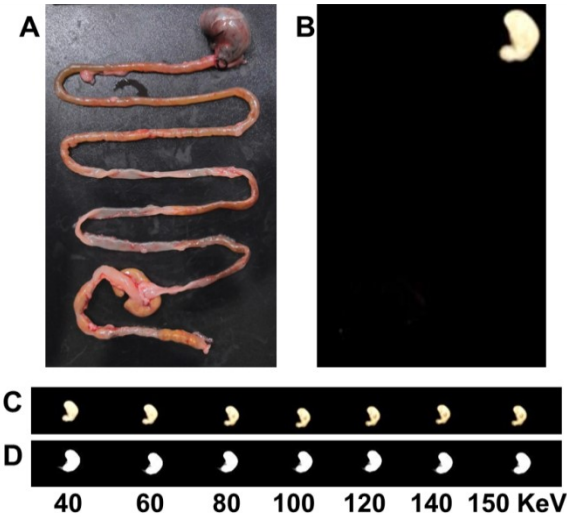

Fig. S10 Picture and spectral CT imaging of the GI tract from the mouse with intestinal obstruction after oral administration of 400 μL of Bi_2S_3 NPs 30 min (Fig. A, Fig. B), the obstruction site was marked with a yellow arrow. Spectral CT imaging of the obstruction site under various X-ray energies (Fig. C is 3-dimensional reconstruction, Fig. D is the coronal image).

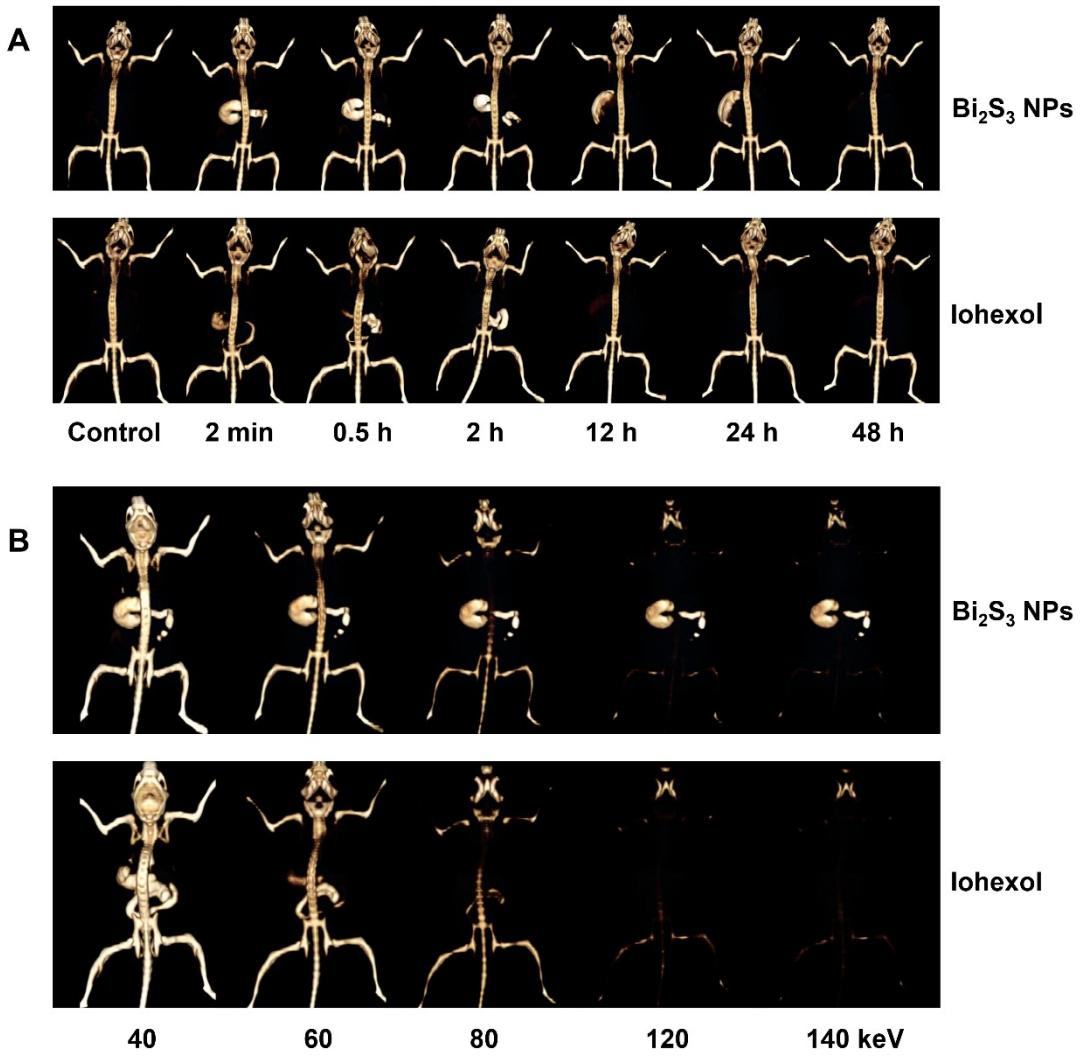

Fig. S11 (A) Traditional CT imaging of GI tract of male mice after orally administration of 550 μL Bi_2S_3 NPs (26 mg/mL Bi_2S_3 NPs, 74.6 mM Bi) or iohexol (20.4 mg/mL iohexol, 74.6 mM I) at 120 kV. (B) Spectral CT imaging of GI tract of male mice at 5 mins after orally administration of 550 μL Bi_2S_3 NPs (26 mg/mL Bi_2S_3 NPs, 74.6 mM Bi) or iohexol (20.4 mg/mL iohexol, 74.6 mM I) at various X-ray energies (40, 60, 80, 120 and 140 KeV).

Table 1 Overview of characteristics of photothermal agents (PCE: Photothermal conversion efficiency；N.A.: Not applicable).

Material	**Size**	**PCE**	**Laser**	**Mass extinction coefficient** L/(g·cm)	**Biological compatibility**	**Ref.**
BSA-Bi_2S_3 nanoparticles	6.1 nm before coating and 39.52 nm after BSA coating	51%	808 nm	2.5 (Bi)	N.A. (in vitro) an acute response of kidney to Bi_2S_3 NPs.	[1]
BSA-coated BiOI@Bi_2S_3	100 nm	28.5%	808 nm	0.18	N.A.(in vitro) Good biosafety (in vivo)	[2]
BSA-CuS nanocrystals	3.7 nm	51.5%	980 nm	12.5 (Cu)	100 μM (cell viability＞80%) Good biosafety (in vivo)	[3]
Cu_2-xS nanocrystals	6.5 nm	16.3%	808 nm	N.A.	50, 6.4, 3.2 mg/L(cell viability＞80% of 4 h, 24 h, 48 h, respectively) High dose of $Cu_{2-x}S$ NCs (100 and 150 mg/kg) led to degenerative necrosis and disappearance of hepatocytes (in vivo).	[4]
Gold nanostar core (Au NCs), MS shell coated with FA	Core: 50 nm; Silica shell: 50-60 nm; Total size: ≈150 nm	31.21 %	808 nm	18.18	57.8 mg/L (HeLa cell viability＞72%, A549 cell viability ＞ 86) Good biosafety (in vivo)	[5]
PEG/ Citrate	PEG@Fe_3O_4:	16.9%	808	10	Fe_3O_4-Cit: 500	[6]

@Fe_3O_4 particles	300 nm Citrate@Fe_3O_4: 240 nm;	(PEG); 15.9% (Citrate)	nm		mg/L (cell viability＞80%) N.A. (in vivo) Fe_3O_4-PEG: 1000 mg/L (cell viability＞80%) N.A. (in vivo)	
Carbon dots	2.9 ± 0.5 nm	38.7%	808 nm	10	N.A. (in vitro and vivo)	[7]
Ultrasmall reduced graphene oxide (nano-rGO)	20 nm	N.A.	808 nm	24.6	10 mg/L (cell viability＞80%) N.A.(in vivo)	[8]
Dopamine - melanin colloidal nanospheres	160 nm	40%	808 nm	2.75	12.5 mg/L (cell viability＞80%) Good biosafety (in vivo)	[9]
Ultrasmall iron oxide - polypyrrole nanoparticles (IONP@ PPy)	100 nm	N.A.	808 nm	30	50 mg/L (cell viability ≈ 100%) Good biosafety (in vivo)	[10]

Reference:

1. Y. Wang, Y. Y. Wu, Y. J. Liu, J. Shen, L. Lv, L. B. Li, L. C. Yang, J. F. Zeng, Y. Y. Wang, L. S. W. Zhang, Z. Li, M. Y. Gao and Z. F. Chai, *Adv. Funct. Mater.,* 2016, **26,** 5335-5344.
2. S. G. Wang, X. Li, Y. Chen, X. J. Cai, H. L. Yao, W. Gao, Y. Y. Zheng, X. An, J. L. Shi and H. R. Chen, *Adv. Mater.*, 2015, **27,** 2775-2782.
3. T. Yang, Y. Wang, H. T. Ke, Q. L. Wang, X. Y. Lv, H. Wu, Y. A. Tang, X. L. Yang, C. Y. Chen, Y. L. Zhao and H. B. Chen, *Adv. Mater.,* 2016, **28,** 5923-5930.
4. S. H. Wang, A. Riedinger, H. B. Li, C. H. Fu, H. Y. Liu, L. L. Li, T. L. Liu, L. F. Tan, M. J. Barthel, G. Pugliese, F. De Donato, M. S. D'Abbusco, X. W. Meng, L. Manna, H. Meng and T. Pellegrino, *ACS Nano*, 2015, **9,** 1788-1800.
5. J. An, X. Q. Yang, K. Cheng, X. L. Song, L. Zhang, C. Li, X. S. Zhang, Y. Xuan, Y. Y. Song, B. Y. Fang, X. L. Hou, Y. D. Zhao and B. Liu, *ACS Appl. Mater. Inter.,* 2017, **9,** 41748-41759.
6. H. B. Peng, S. W. Tang, Y. Tian, R. Zheng, L. Zhou and W. L. Yang, *Part. Part. Syst. Char.*, 2016, **33,** 332-340.
7. M. Zheng, Y. Li, S. Liu, W. Q. Wang, Z. G. Xie and X. B. Jing, *ACS Appl. Mater. Inter.,* 2016, **8,** 23533-23541.

8. J. T. Robinson, S. M. Tabakman, Y. Y. Liang, H. L. Wang, H. S. Casalongue, D. Vinh and H. J. Dai, *J AM Chem. Soc.*, 2011, **133,** 6825-6831.
9. Y. L. Liu, K. L. Ai, J. H. Liu, M. Deng, Y. Y. He and L. H. Lu, *Adv. Mater.,* 2013, **25,** 1353-1359.
10. X. J. Song, H. Gong, S. N. Yin, L. Cheng, C. Wang, Z. W. Li, Y. G. Li, X. Y. Wang, G. Liu and Z. Liu, *Adv. Funct. Mater.*, 2014, **24,** 1194-1201.